GEOCHEMISTRY

# Extreme variability in atmospheric oxygen levels in the late Precambrian

**Alexander J. Krause[1,2]*, Benjamin J. W. Mills[1], Andrew S. Merdith[1,3], Timothy M. Lenton[4], Simon W. Poulton[1]**



**Mapping the history of atmospheric $O_2$ during the late Precambrian is vital for evaluating potential links to animal evolution. Ancient $O_2$ levels are often inferred from geochemical analyses of marine sediments, leading to the assumption that the Earth experienced a stepwise increase in atmospheric $O_2$ during the Neoproterozoic. However, the nature of this hypothesized oxygenation event remains unknown, with suggestions of a more dynamic $O_2$ history in the oceans and major uncertainty over any direct connection between the marine realm and atmospheric $O_2$. Here, we present a continuous quantitative reconstruction of atmospheric $O_2$ over the past 1.5 billion years using an isotope mass balance approach that combines bulk geochemistry and tectonic recycling rate calculations. We predict that atmospheric $O_2$ levels during the Neoproterozoic oscillated between ~1 and ~50% of the present atmospheric level. We conclude that there was no simple unidirectional rise in atmospheric $O_2$ during the Neoproterozoic, and the first animals evolved against a backdrop of extreme $O_2$ variability.**

## INTRODUCTION

It is widely believed that atmospheric oxygen rose across three broad steps during the course of Earth's 4.5-billion-year history (*1*–*4*). The first of these steps—the Great Oxidation Episode (GOE)—occurred from ~2.43 to 2.22 billion years (Ga) ago (*5*), and key pieces of geological and geochemical evidence indicate a permanent state change (see Fig. 1). The loss of mass-independent sulfur isotope fractionation (MIF-S) (*6*) suggests that $O_2$ levels after the GOE remained above at least $10^{-6}$ present atmospheric level (PAL) (i.e., 0.0001% PAL) but were likely several orders of magnitude higher (*7*, *8*), while the rise of terrestrial red beds and the loss of detrital pyrite and uraninite in fluvial sediments point to $O_2$ > 1% PAL (*9*–*11*). Similarly, during the third step—the Paleozoic Oxygenation Event (POE)—which occurred from ~450 to 400 million years (Ma) ago (*1*, *2*), a substantial increase in the abundance of sedimentary charcoal (*12*) as well as accompanying step changes in cerium anomalies (*13*) and the oxidation state of marine basalts (*14*) all point to a stepwise increase in oxygen levels from <50% PAL to >66.5% PAL.

There is substantial debate, however, over the timing and tempo of the second $O_2$ step—the Neoproterozoic Oxygenation Event (NOE) (*15*)—and it appears increasingly likely that the early hypothesis (*4*) of a stepwise change to near-modern $O_2$ levels at this time is not correct (*1*, *2*). A stepwise shift towards a new stable $O_2$ level during the NOE has not been ruled out but is somewhat difficult to reconcile with the dynamic nature of the Earth system during this time period, which included two "Snowball Earth" glaciations (the Sturtian at ~717 to 659 Ma and the Marinoan at ~649 to 635 Ma) and their "super-greenhouse" aftermaths (*16*–*20*), as the supercontinent Rodinia fractured into a multitude of low-latitude microcontinents (*21*).

Meanwhile, terrestrial proxies provide conflicting lines of evidence as to atmospheric $O_2$ levels during the run-up to the NOE (i.e., the later Mesoproterozoic and early Neoproterozoic), making it difficult to define an $O_2$ threshold that must have been crossed, which contrasts with the GOE and its associated MIF-S record. A lack of chromium isotope ($\delta^{53}Cr$) fractionation, where greater fractionation from the bulk silicate Earth (BSE) pool is indicative of oxidative weathering of Cr (*22*–*24*), has been interpreted to imply $O_2$ levels of <0.1% PAL before 800 to 750 Ma (*23*, *24*). This level is based on the assumption that Cr oxidation is dependent on the amount of time that Cr spends in a weathering environment in close contact with $O_2$ (*23*). However, other work (*8*) has shown that the weathering horizon beneath the upper soil layers (i.e., below a depth of ~1 m) may have been anoxic, and therefore $O_2$ exposure during fluvial transport to the oceans was potentially more important for oxidative Cr weathering, implying an $O_2$ level of ~10% PAL. Furthermore, more recent analyses using $\delta^{53}Cr$ have indicated extensive isotopic fractionation and therefore $O_2$ concentrations of >0.1% PAL before the NOE (*25*, *26*). In addition, the appearance of terrestrial red beds suggests $O_2$ concentrations of >1% PAL since the GOE (*11*), while constraints from the mass-independent fractionation of oxygen isotopes suggest an atmospheric $O_2$ concentration of ~0.34% PAL at ~1400 Ma (*27*). In the marine realm, redox-sensitive trace elements (RSEs) suggest the possibility of $O_2$ concentrations above ~4% PAL as early as 1400 Ma (*28*).

Marine geochemical proxies do not appear to agree on resilient oceanic oxygenation during the Neoproterozoic. The I/(Ca + Mg) proxy, which is thought to track the extent of upper ocean oxygenation, suggests relatively low $O_2$ levels throughout the Neoproterozoic Era, with a temporary rise at ~800 Ma (*29*, *30*). In turn, interpretation of cerium anomalies suggests that a modern level of ocean oxygenation was not reached until the Devonian (*13*, *31*), while uranium isotopes ($\delta^{238}U_{sw}$)—which are considered to reflect global trends in ocean redox—suggest that the ocean experienced multiple oxygenation events across the Cryogenian, Ediacaran, and Cambrian (*32*). Such fluctuations are in general agreement with Se isotope systematics (*33*) and RSEs in black shales (*34*), as well as iron speciation analyses that point to spatially and temporally restricted episodes of deep ocean oxygenation (see Fig. 1B) (*35*, *36*). Thus, a complex picture of variability in the extent of ocean oxygenation during the Neoproterozoic has emerged. Furthermore, changes to the redox state of the ocean interior are not necessarily tied to $O_2$ levels in the atmosphere

[1]School of Earth and Environment, University of Leeds, Leeds LS2 9JT, UK. [2]Department of Earth Sciences, University College London, 5 Gower Place, London WC1E 6BS, UK. [3]Laboratoire de Géologie de Lyon: Terre, Planète, Environnement, UMR CNRS 5276, Université Claude Bernard, Lyon1, 2, rue Raphaël Dubois, 69622 Villeurbanne Cedex, France. [4]Global Systems Institute, University of Exeter, Exeter EX4 4QE, UK.
*Corresponding author. Email: a.krause@ucl.ac.uk

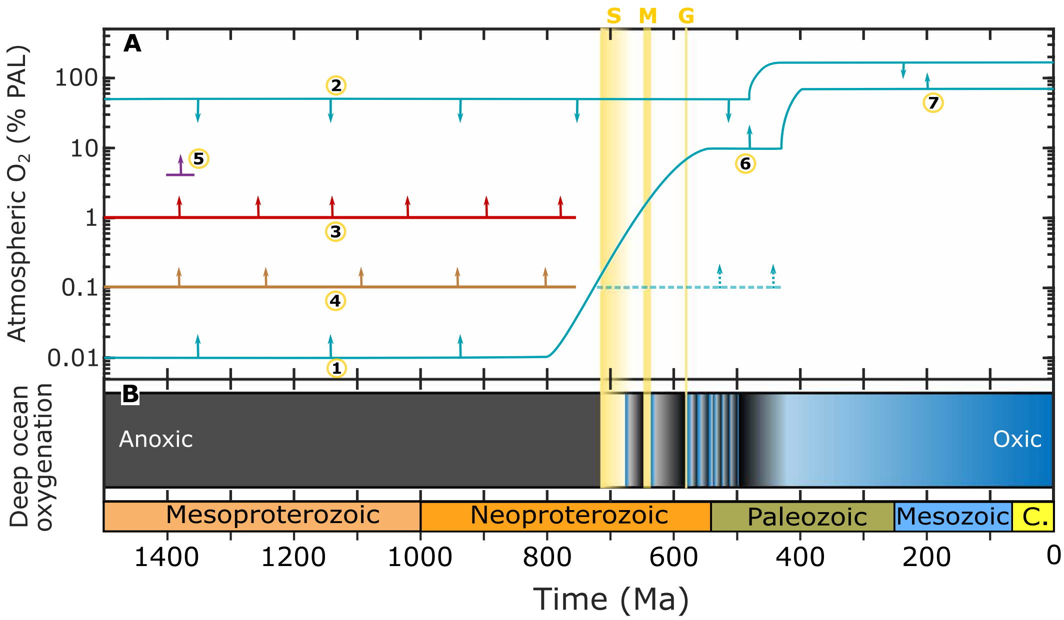


**Fig. 1. Current "best guess" estimates for atmospheric oxygen evolution over the past 1500 Ma and deep ocean oxygenation based on multiple geochemical proxy records.** (**A**) Current generalized view of atmospheric oxygen levels since 1500 Ma (*4*) and (**B**) deep ocean oxygenation [where the black represents anoxia in the deep ocean, and the blue lines are oceanic oxygenation events (OOEs) as inferred from global marine proxies such as $\delta^{238}U$ and RSEs, grading to a fully oxic ocean at present day] (*32*, *34*). The numbered circles in (A) denote the following: (1) a lower boundary for $O_2$ based on the loss of the MIF-S ($O_2$ > 0.0001% PAL) (*6*, *7*) but minimal $\delta^{53}Cr$ fractionation ($O_2$ < 0.1% PAL) (*23*, *24*), (2) an upper limit of <50% PAL until ~420 Ma based on geochemical water column redox data and allowing for modeling uncertainties (*42*, *83*, *84*), (3) the appearance of terrestrial red beds and loss of detrital pyrite and uraninite (*11*), (4) instances of significant $\delta^{53}Cr$ fractionation during the Mesoproterozoic ($O_2$ > 0.1% PAL) (*25*, *26*), (5) RSE data indicating $O_2$ > ~4% PAL at 1400 Ma (*28*), (6) likely minimum $O_2$ (>10% PAL) required by late Ediacaran and Cambrian biota (*85*), and (7) both upper and lower $O_2$ limits for the past 420 Ma based on the wildfire record from sedimentary charcoal abundance and modeling studies (*12*, *86*). Yellow bands represent the two potential "Snowball Earth" glaciations ("S", Sturtian and "M", Marinoan) and the later ("G", Gaskiers) glaciation of the Neoproterozoic.

and surface ocean, leading to major uncertainty in terms of oxygen controls on metazoan evolution.

## Isotope mass balance

Here, we use an isotope mass balance approach to directly infer atmospheric oxygen concentrations from 1500 Ma to the present day. This approach was first developed in the 1980s (*37*) and was subsequently used to build the GEOCARBSULF model for estimating Phanerozoic $O_2$ concentrations (*38*). Isotope mass balance uses the isotopic composition of sedimentary material, alongside major tectonic material fluxes, to estimate the source and sink fluxes in the geological oxygen cycle (which comprise the burial of organic carbon and pyrite sulfur and their weathering and tectonic recycling).

Few isotope mass balance studies have been performed for the Precambrian, and these have tended to focus on the operation of the carbon cycle in general, rather than attempting to produce a quantitative estimate of $O_2$ (*39*, *40*). Previous predictions of $O_2$ in the late Neoproterozoic to early Cambrian using the GEOCARBSULF framework (*41*) have produced sustained high $O_2$ levels (much greater than the 21% of the present-day atmosphere by volume), contrary to evidence for widespread deep ocean anoxia (*42*), and consequently have hitherto presented a challenge for applying this approach to earlier Earth history. Given these difficulties, other experimental numerical methods have been used to attempt to reconstruct Precambrian oxygen levels through comparison to redox-sensitive element concentrations or fluid inclusion measurements (*43*–*45*), but both of these methods violate very robust limits set by either the MIF-S signal or the presence of wildfires, by an order of magnitude or more.

Recent work using GEOCARBSULF identified that unfeasibly strong constraints within the sulfur cycle prevented the model from predicting low (<50% PAL) $O_2$ levels in the early Paleozoic (*2*). Recognizing this limitation, a rewriting of the GEOCARBSULF model from first principles, using a "forwards" approach to the sulfur cycle (termed GEOCARBSULFOR), predicts low $O_2$ in the early Paleozoic (*2*). Here, we build upon this updated methodology and show that isotope mass balance can be used to predict atmospheric $O_2$ levels in the Precambrian, despite the extreme variations evidenced in the $\delta^{13}C$ record, using a framework we call NEOCARBSULF.

The major equations for isotope mass balance are derived from the assumption that, at steady state, the total mass of each isotope of carbon (or sulfur) must be conserved; thus

$$\delta^{13}C_{in} = \delta^{13}C_{org} f_{org} + \delta^{13}C_{carb}(1 - f_{org}) \quad (1)$$

where $\delta^{13}C_{in}$ is the $^{13}C$ to $^{12}C$ ratio of carbon inputs (e.g., from metamorphism and weathering); $C_{org}$ and $C_{carb}$ represent organic carbon and carbonate, respectively; and $f_{org}$ is the fraction of carbon buried as organic carbon. Knowledge of the biological isotopic fractionation imparted by photosynthesis ($\Delta C$) and the total carbon input (i.e., the sum of all weathering and degassing fluxes for both $C_{carb}$ and $C_{org}$) to the combined ocean-atmosphere reservoir ($F_{total}$) allows Eq. 1 to be recast in the form

$$F_{bg} = \frac{F_{total}(\delta^{13}C_{carb} - \delta^{13}C_{input})}{\Delta C} \quad (2)$$

where $F_{bg}$ is the burial rate of organic carbon, representing the major source of $O_2$ over geological time scales. The weathering and burial of carbonates are accounted for in these isotope mass balance equations, and we also include the effect of erosion on carbonate weathering (see Materials and Methods), which affects the link between the $\delta^{13}C$ record and $O_2$ production (*46*). Oxidizing power can also be produced by the long-term sulfur cycle through the burial of pyrite. Following Phanerozoic modeling, our approach calculates pyrite burial rates from a combination of sulfate availability, organic carbon availability, and the model-predicted marine redox state (*2*).

To calculate the total carbon input rate ($F_{total}$), we reconstruct the weathering and degassing/metamorphic fluxes for both organic carbon and carbonates (see Materials and Methods for further details) to reflect an increasing crustal carbon inventory and recycling rate. Seafloor weathering is not included, although it is an important component in process-driven Precambrian modeling (*47*) primarily due to its effect on the phosphorus supply for primary productivity. It is less important here because organic carbon burial is calculated directly through isotope mass balance rather than nutrient availability.

The isotope mass balance model was run 5000 times, with 18 parameters sampled from well-defined limits (see Materials and Methods and the Supplementary Materials), to account for the uncertainty of key variables. The key input parameters are shown in Fig. 2 and comprise the $\delta^{13}C$ record (Fig. 2A), tectonic degassing rates (Fig. 2B), and mountain uplift (Fig. 2C), which affect the burial, degassing, and weathering fluxes of carbon and sulfur, respectively, and an increasing crustal carbon inventory over time (Fig. 2D), all of which can alter the predictions for $O_2$. We also explore uncertainty in how the difference between the $\delta^{13}C$ of inorganic carbon ($\delta^{13}C_{carb}$) and $\delta^{13}C$ of organic carbon ($\delta^{13}C_{org}$) may have changed over the past 1500 Ma and the effect of this difference on $O_2$ predictions (see Materials and Methods). The first version of the GEOCARBSULF model (*38*) used the paired $\delta^{13}C_{carb}$ and $\delta^{13}C_{org}$ records to calculate C isotope fractionation during photosynthesis, but subsequent iterations [e.g., (*2*, *41*, *48*, *49*)] use an $O_2$-dependent equation to derive C isotope fractionation. Here, we use both approaches to drive the model as part of the uncertainty analysis. We do not include all of the model input parameters (e.g., different present-day rates or fluxes) in our Monte Carlo analysis, as previous work (*48*) has shown that their inclusion does little to affect the mean $O_2$ output, and as previously noted (*38*, *49*), atmospheric $O_2$ levels are predominately affected by the burial, rather than weathering, fluxes in the model.

Our model includes an assumed pulse of gypsum burial in the Tonian (Fig. 2E) and its later weathering and conversion to pyrite in the Ediacaran (Fig. 2F), which is thought to be responsible for the Shuram-Wonoka sustained negative carbon isotope anomaly (*50*). Functionally, this prevents the model outputting negative $O_2$ during the Shuram, where the carbon isotope record suggests that the C cycle became a net sink for $O_2$.

## RESULTS

We plot the $O_2$ results from NEOCARBSULF (Fig. 3) from 1500 Ma, disregarding a 100 million year model spin-up time from 1600 to 1500 Ma. The results (Fig. 3B) show a regime change in $O_2$ levels during the Neoproterozoic and again during the Paleozoic. NEOCARBSULF predicts a small (<10% PAL) and unstable atmospheric $O_2$ inventory during the Mesoproterozoic, with the potential for drops to very low levels, although poor data density in the $\delta^{13}C$ record prevents any clear documentation of these shifts. The overall trend is a rise in $O_2$ levels from ~1500 to ~750 Ma, albeit in an oscillating fashion. Predicted $O_2$ levels then begin to decline, with an eventual return to the low levels of the Mesoproterozoic as the Earth entered the Sturtian glaciation. During the interglacial, $O_2$ rises to ~50% PAL before dropping again as the Earth entered the Marinoan glaciation. Post-Marinoan atmospheric $O_2$ exhibits rapid variability across most of the Ediacaran and Cambrian periods. Another low is recorded during the early Ordovician (485.4 to 470 Ma), before $O_2$ begins its inexorable rise to modern-day levels at the end of the Ordovician, in agreement with earlier work using isotope mass balance calculations (*2*).

## DISCUSSION

We have produced the first quantitative reconstruction of atmospheric $O_2$ levels during the entire Neoproterozoic. Crucially, our modeling suggests that $O_2$ levels were highly variable, changing by an order of magnitude within just a few tens of million years, and that a more permanent rise to modern-day $O_2$ levels did not occur until the Paleozoic. These highly dynamic results for atmospheric $O_2$ in the Neoproterozoic appear to be a better match to geochemical proxy data than a simple stepwise increase in atmospheric $O_2$. First, our model predicts elevated $O_2$ levels of >13% PAL for ~85 million years, from 900 to 815 Ma, which corresponds to a baseline shift in $\delta^{53}Cr$ fractionation in 900- to 800-Ma aged shales (*24*). Furthermore, $\delta^{238}U_{sw}$ values at the onset of the Bitter Springs C isotope excursion (810 Ma) (*51*) are below that of modern seawater, indicating widespread anoxia at a time when our results suggest that $O_2$ was in temporary decline (*52*). Oxygen levels then start to recover at 803 Ma, as the negative isotope excursion ends, which is consistent with increased I/(Ca + Mg) ratios signifying enhanced upper ocean oxygenation at this time (*30*). Meanwhile, $\delta^{53}Cr$ data suggest a rise in $O_2$ at ~750 Ma (giving a sizeable fractionation from the BSE) (*24*), consistent with our results indicating $O_2$ levels of ~50% PAL.

NEOCARBSULF predicts that $O_2$ decreased at the onset of the Sturtian glaciation (Fig. 3), consistent with the implication that glacial advance would have restricted the flux of nutrients and sunlight to the ocean, leading to a collapse in primary productivity (*16*). Our results suggest that $O_2$ recovered after the Sturtian, in agreement with $\delta^{238}U_{sw}$ data from carbonates deposited at the termination of the glaciation, recording an average value (−0.47‰), which is not dissimilar to that of modern seawater (−0.39 ± 0.01‰) (*32*). When coupled with box modeling (*32*), this suggests extensive, albeit temporary, seafloor oxygenation before the Earth began its descent into the Marinoan glaciation, whereupon NEOCARBSULF $O_2$ levels begin to decline and the $\delta^{238}U_{sw}$ average drops (to ~−0.70‰) (*53*).

For ~8 million years during the Marinoan, our mean results fall into the $O_2$ range of $3 \times 10^{-6}$ to 1% PAL, where photochemical modeling suggests that few stable solutions exist (*54*); thus, $O_2$ would crash to levels below $3 \times 10^{-6}$ PAL, in conflict with the geological record. However, specific dynamics associated with the glaciation may be in play here. NEOCARBSULF has a simple albedo function to affect temperature predictions; thus, for the Marinoan and the Sturtian, it is possible that we have missed more rapid or extreme fluctuations in $O_2$, $CO_2$, and temperature, or stabilizing feedbacks, which may have dampened such changes. This could be tested in the future by coupling NEOCARBSULF to an ice-albedo model. This may also help to improve the ±1 SD solution space of NEOCARBSULF for the whole 1500 million year time frame.

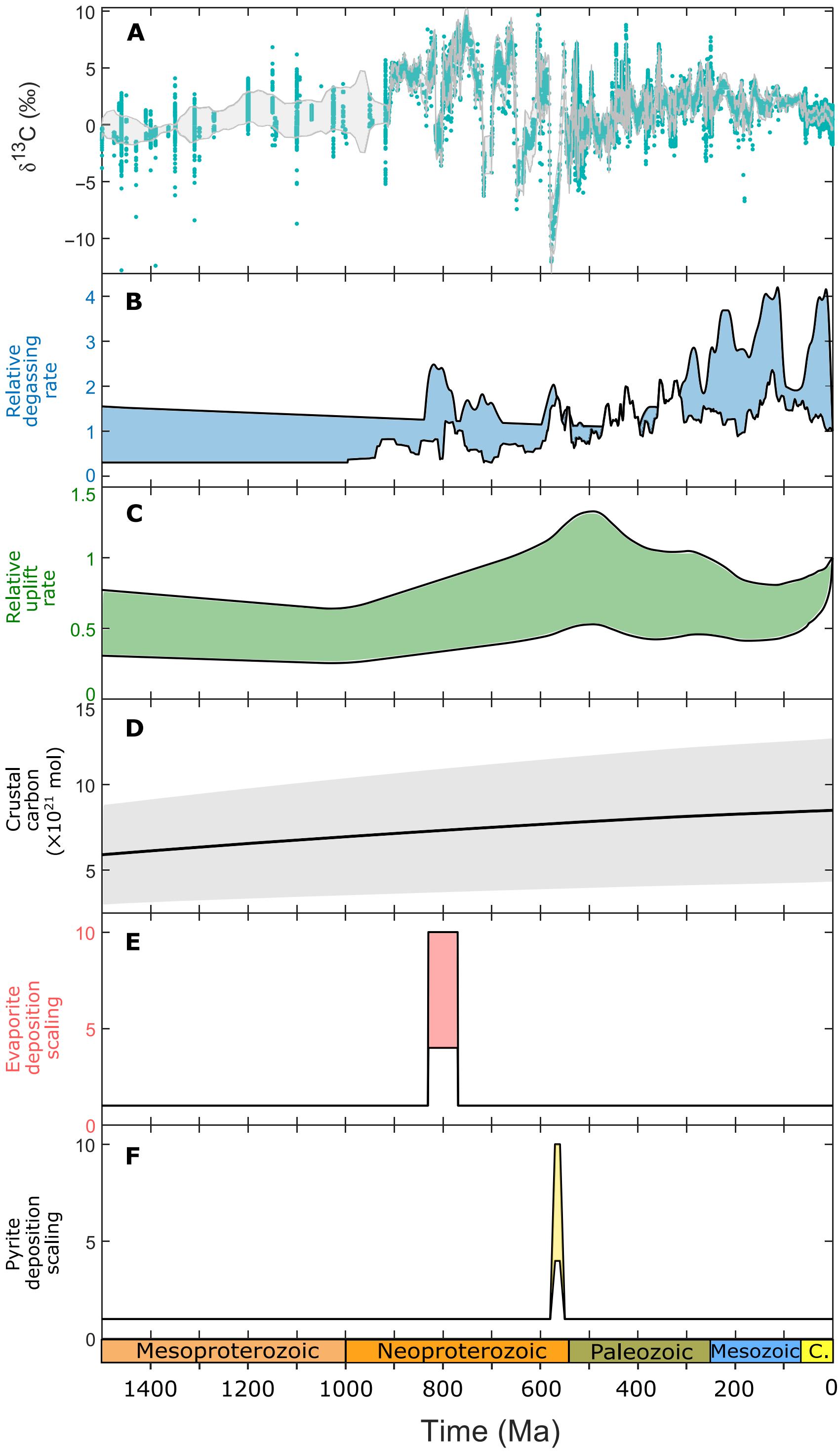


**Fig. 2. Key parameters in the NEOCARBSULF model.** (**A**) Compilation of $\delta^{13}C$ through time (teal dots), with the gray band representing ±1 SD of a moving average. The data are taken from previous compilations (*67*, *68*) and references therein. (**B**) Tectonic degassing, normalized to the present day, where the black boundaries represent the Monte Carlo sampling limits. (**C**) Mountain uplift, normalized to the present day, where the black boundaries represent the Monte Carlo sampling limits. (**D**) Increase in the crustal carbon reservoir since 1500 Ma (*79*). (**E**) Scaling factor introduced into the model to simulate large-scale evaporite deposition in the Tonian. (**F**) Scaling factor introduced to replicate a proposed increase in pyrite burial coincident with the Shuram-Wonoka anomaly. See Materials and Methods for further details.

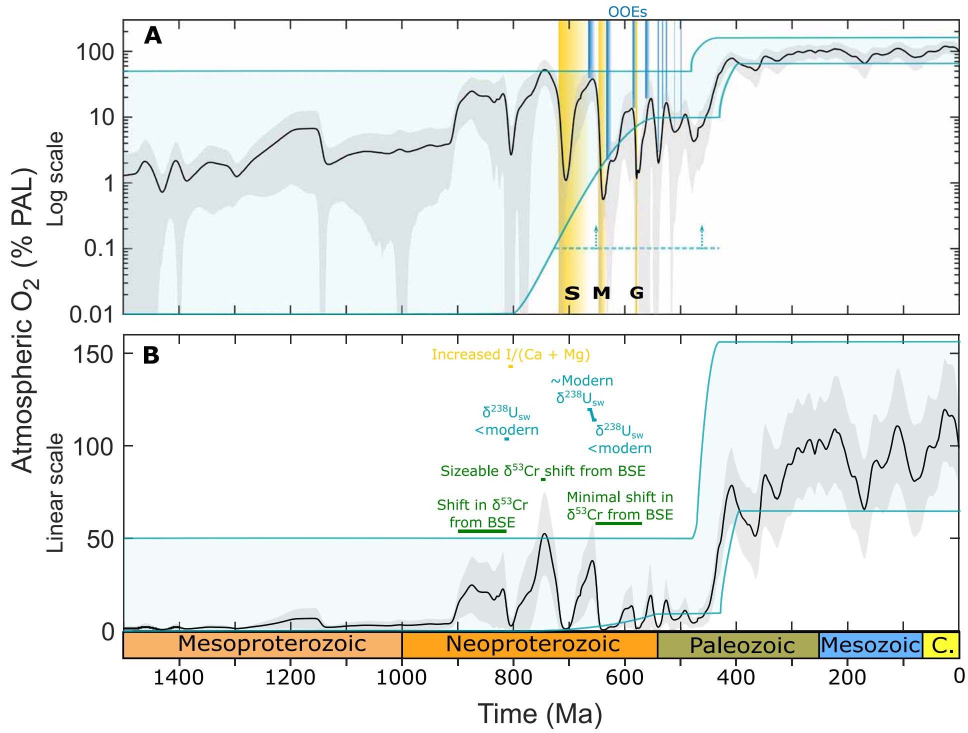


**Fig. 3. Reconstructed $O_2$ evolution from 1500 Ma to present.** Atmospheric oxygen results estimated from the NEOCARBSULF model in log (**A**) and linear (**B**) forms. In each panel, the black line is the mean result of 5000 model runs, and the gray shaded band represents ±1 SD, which may include very low values on occasion. The blue shaded band is the $O_2$ best guess estimate from Fig. 1A (top panel). In (A), the blue lines are the OOEs as seen in Fig. 1B (bottom panel). The blue dashed line with arrows is the minimum $O_2$ level previously defined by substantial $\delta^{53}$Cr fractionation (*23*, *24*). The yellow lines are the glaciations: S, Sturtian; M, Marinoan; G, Gaskiers. In (B), notable geochemical proxies—see text for further details.

Atmospheric $O_2$ does recover after the Marinoan, which can be tracked by the enrichment of RSEs in shales at this time (*34*), but the comparatively slower speed of its recovery correlates with minimal $\delta^{53}$Cr variation from the BSE value that is observed until 570 Ma (*24*).

Isotope mass balance predicts that $O_2$ levels were also unstable in the Ediacaran and early Cambrian but with variability across a narrower range of between ~1 and ~20% PAL (Fig. 3). In general, NEOCARBSULF predictions of rises (or high levels, compared to the rest of this time frame) in $O_2$ in the Ediacaran and Cambrian are in agreement with RSE enrichments (*34*) at ~580, ~560, ~535, and ~525 Ma. The only exception is where the RSE data predict an oceanic oxygenation event at ~540 Ma, when NEOCARBSULF indicates temporarily low $O_2$ (~2% PAL) based on declining $\delta^{13}$C values. However, rapid inputs of other oxidants such as sulfate could have maintained or even expanded the $O_2$ reservoir (*50*) for shorter periods. We follow previous work (*50*) in inputting a large pulse of sulfate coincident with the >10 million year Shuram negative carbon isotope excursion (see Materials and Methods), where there is evidence for the exposure of Tonian-aged evaporite deposits. This prevents deoxygenation in the model during the Shuram, when the $\delta^{13}$C record suggests net oxidation of organic carbon. It is possible that we have missed other sulfate inputs during the Neoproterozoic to Cambrian, given that evaporite dissolution leaves no clear signal in the rock record. Given the lack of evidence for long-lived net C oxidation pre-Shuram, these sulfate inputs would likely have been much smaller, and thus may have resulted in only minor increases in atmospheric $O_2$ compared to our model predictions.

Although the interpretation of the Shuram excursion remains contentious, with various authors suggesting that such a deeply negative signal must be the result of either authigenic cements (*55*), localized phenomena (*56*), or diagenetic alteration (*57*), recent work has documented the globally synchronous nature of the event (*50*) and finds no evidence of late diagenetic overprinting (*58*). Regardless, we capture some of the uncertainty around the $\delta^{13}$C record within our Monte Carlo sampling approach. Generally speaking, the predicted variability in atmospheric $O_2$ across the Ediacaran and Cambrian suggests that fluctuating oxygen levels, rather than progressive oxygenation of the oceans, accompanied the Cambrian explosion (*59*).

Our biogeochemical framework allows us to test the robustness of our oxygen results by making predictions for other Earth system metrics with known quantities. In Fig. 4, we compare these model outputs to various geochemical proxies and other kinds of modeling studies. Our model $CO_2$ predictions (Fig. 4A) show good agreement with the proxy window for the majority of the past ~420 million years, with the mean of model runs lying within, or very close to, the proxy window. The decline of $CO_2$ across the Ordovician through to the Devonian is in close association with the rise in $O_2$ across this time frame and is linked to the evolution of land plants in the model (*38*), which draw down atmospheric $CO_2$ while simultaneously increasing the total carbon throughput to the ocean-atmosphere system.

The notable disagreements between our $CO_2$ results and the proxy record are during the end of the Early Cretaceous and much of the Late Cretaceous (~117 to 74 Ma), where the model follows the general trend of declining $CO_2$ but predicts values much lower than the proxy record. The root cause of this may be that degassing rates based on rift lengths alone are very high in the Early Cretaceous but decrease sharply toward the end of this Epoch, while spreading rates based on subduction zone lengths experience only a minor decline. This results in a skewing of the Monte Carlo simulation, generating a modeled Earth system with higher $CO_2$ and thus temperature (see fig. S2), earlier in the Cretaceous, than would otherwise be predicted if NEOCARBSULF used the sea-level inversion degassing rates from previous GEOCARB(SULF) modeling (*38*, *48*, *60*).

Our $f_{pyr}$ output (Fig. 4B)—the fraction of sulfur leaving the ocean as pyrite—is a reasonable fit to the record, whereby the model generally predicts fairly high (~0.75) pyrite burial in the Precambrian. The exception to this is a period of sustained gypsum deposition between 830 and 770 Ma, which has been imposed on the model in light of evidence for substantial deposition of evaporites in the Tonian, which were later weathered during the Ediacaran (see Materials and Methods) (*50*). Our mean (black line) Phanerozoic predictions are very close to previous modeling (*61*), apart from $f_{pyr}$ values that are slightly lower in the late Cambrian–early Ordovician and slightly higher during the Triassic (but are mostly encapsulated within the ±1 SD range). Our model output for the ocean sulfate reservoir (Fig. 4C) captures the long-term trend of increasing sulfate concentration over the past 1500 million years and correlates to a number of fluid inclusion data points and prior modeling efforts (*62*). Finally, instead of inverting the $\delta^{34}S$ record to help derive pyrite burial as per the original GEOCARBSULF (*38*), NEOCARBSULF can predict the global $\delta^{34}S$ record through time. Our model estimates (Fig. 4D) match the geological record reasonably well. The clearest area of mismatch is the Cryogenian, where $\delta^{34}S$ is lower than in the geological record by around 10‰, but $f_{pyr}$ is broadly in agreement. However, the long-term trend remains robust. Other model outputs are compared to geological data in the Supplementary Materials and are also in general agreement.

In agreement with earlier isotope mass balance modeling, our qualitative variations in atmospheric $O_2$ are largely inferred from fluctuations in carbonate $\delta^{13}C$, from which we infer organic carbon burial. While the link between $\delta^{13}C$ and calculated organic carbon burial may be altered by changes to the inorganic carbon cycle (*46*), these changes are not well known on sub–~100 million year time scales during the Neoproterozoic. Changes to erosion rates, due to either supercontinent cycles or extensive glaciation, may have altered the supply of nutrients to the oceans through the Neoproterozoic, which may have helped drive the large fluctuations in organic carbon burial that our model predicts. Testing this hypothesis requires the use of a forwards model instead, which contains a system for calculating organic carbon burial rates based on nutrient availability and other Earth system processes and can potentially be validated against the $\delta^{13}C$ record.

A key advance in our work over previous attempts to apply isotope mass balance to the Precambrian [e.g., (*44*)] is the assessment of overall carbon cycling rates through a combination of degassing, uplift, and crustal carbon storage. Here, it emerges that a key aspect driving our prediction is the overall increase in crustal carbon storage and tectonic recycling rate over Earth history. Traditionally, there has been something of a paradox surrounding the long-term stability of $\delta^{13}C$ around 0‰, which indicates that the fraction of carbon buried organically (and therefore the key $O_2$ source) did not see any long-term increase or decrease (*63*), which has been seen as contradictory to increasing levels of atmospheric $O_2$. Here, we confirm that this long-term $\delta^{13}C$ stability can be maintained in tandem with rising $O_2$ levels because the total rate of carbon cycling is increasing, which adds to the currently understood feedback through oxygen-dependent



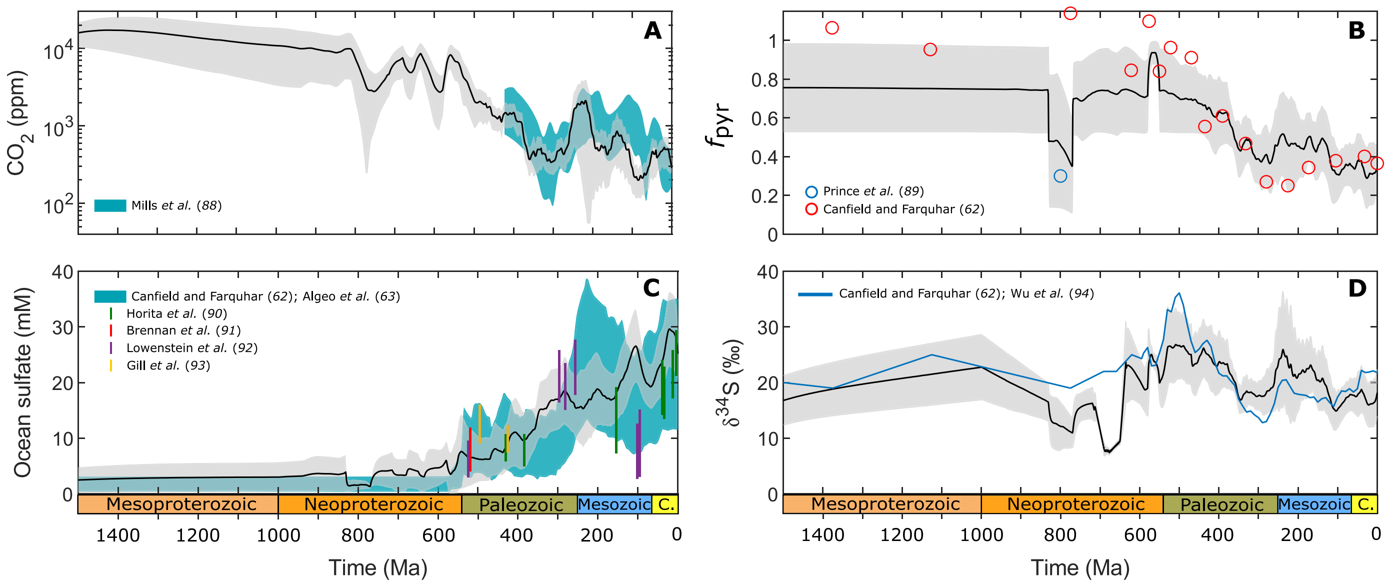


**Fig. 4. Additional outputs from the NEOCARBSULF model compared to geochemical data and other modeling studies.** For all panels, the black line is the mean result of 5000 model runs, and the gray window represents ±1 SD. (**A**) Atmospheric $CO_2$ predictions compared to a compilation of geochemical proxies (blue band) for the past 420 million years (*87*). ppm, parts per million. (**B**) Fraction of total sulfur burial that is in the form of pyrite, compared to modeling of $\delta^{34}S$ data (*61*, *88*). (**C**) Sulfate concentration of the ocean over time. The blue band represents the ±1 SD uncertainty range of previous reconstructions (*61*, *62*), and the vertical colored bands are values based on fluid inclusion studies or modeling (*89*–*92*). (**D**) Modeled prediction of the global average $\delta^{34}S$ record through time, compared to geochemical data (*61*, *93*).

weathering of organic matter (and associated input of isotopically light carbon) (*8*). In addition to this mechanism, the evolution of land plants, particularly deep-rooted vascular plants in the Paleozoic, likely facilitated a substantial increase in the total carbon input via enhanced carbonate weathering (*64*), meaning that small variations in the $\delta^{13}C$ record from the late Paleozoic onwards, are capable of producing large changes in atmospheric $O_2$.

Our results predict that, while there was a fundamental change in the oxygen cycle in the Neoproterozoic leading to some form of NOE (*15*), this was not a unidirectional step change, but rather a series of oxygen oscillations. Although fluctuations in marine $O_2$ levels during the Neoproterozoic have been inferred from a multitude of sedimentary geochemical proxies, our study provides the first clear quantitative evidence for highly variable atmospheric $O_2$ levels in the late Proterozoic. Such variations in $O_2$ were likely in response to the global tectonic regime during the Cryogenian-Cambrian, as the supercontinent Rodinia broke apart (ca. 800 to 600 Ma) and Gondwana began to coalesce (ca. 650 to 500 Ma), and was exacerbated by internal feedbacks within the oxygen cycle (*3*). Our results are consistent with the hypothesis that the evolution of land plants was the key event that ultimately stabilized oxygen at near-modern levels, paving the way for the evolution of marine animals with a much higher $O_2$ demand (e.g., large predatory fish) (*65*) and, eventually, animal life in the terrestrial realm. In contrast, our results here suggest that the first marine animals evolved amidst a backdrop of fluctuating global oxygen levels.

## MATERIALS AND METHODS

### Model overview

The NEOCARBSULF model is an extension of GEOCARBSULFOR (*2*) and is solved in MATLAB using an implicit variable-order ordinary differential equation (ODE) method (*66*). The original GEOCARBSULF model (*38*) was solved using an Euler approach, but the differential equations used by the model are "stiff"; therefore, there is a high degree of numerical instability, which sometimes leads to model failure when using explicit methods with set step sizes (*48*). GEOCARBSULFOR was built to use the ODE15s solver in MATLAB, which permits (among other things) a dynamic step size, allowing the model to adapt to areas of stiffness when solving the equations, and we continue to use this solver in NEOCARBSULF. The full set of model equations and information about the data used can be found in tables S1 to S7.

### The $\delta^{13}C$ record and $\delta^{13}C$ fractionation

The $\delta^{13}C$ record is updated to use data from (*67*) for the Mesoproterozoic and early Tonian and from (*68*) for the rest of the Neoproterozoic and Phanerozoic. To these data, we applied a 10 million year moving average with smoothing to eliminate variations over very short time scales and obtained a ±1 SD for our Monte Carlo analysis.

The GEOCARBSULF and GEOCARBSULFOR models (*2*, *38*) use an $O_2$-dependent equation to calculate $\delta^{13}C$ fractionation ($\Delta^{13}C$), which is based on plant and plankton growth experiments under different atmospheric $O_2$ concentrations (*69*, *70*). This equation (eq. S25 in table S6) includes the present-day $\Delta^{13}C$ and a curve-fitting parameter (*J*). The present-day $\Delta^{13}C$ has a ~6‰ range (*71*), and while *J* is reasonably approximated for much of the Phanerozoic (after the evolution of land plants), the value of *J* in the Precambrian is uncertain. An alternative approach would be to use $\Delta^{13}C$ data based on the paired records of $\delta^{13}C_{carb}$ and $\delta^{13}C_{org}$, such as that previously compiled (*71*). However, the resolution of the $\delta^{13}C_{org}$ record in particular is coarse and thus requires binning of the data on 10 million year time scales, which misses geologically rapid (~1 million year) variations. Furthermore, non-marine $\delta^{13}C$ data are excluded from the statistical analysis (*71*), but this may be problematic for reconstructing $O_2$ from the mid-Paleozoic onwards, as terrestrial organic matter generally has a different $\delta^{13}C$ signature to that found in marine settings, which reflects a mixture of both marine and terrestrial organic matter (*38*).

As there are substantial uncertainties with either approach, we combine the two by including the present-day $\Delta^{13}C$, *J*, and the maximum and minimum bounds of the Kalman smoothed $\Delta^{13}C$ data (*71*) into our Monte Carlo simulation. The model calculates a $\Delta^{13}C$ value at each time step using the equation approach and separately picks a $\Delta^{13}C$ value from in between the Kalman bounds. The two values are combined and then averaged (see eq. S26), providing a midpoint value between the two approaches, and this $\Delta^{13}C$ value is used for calculating organic carbon burial (eqs. S29 and S30).

### Uplift and erosion

In the original GEOCARBSULF model (*38*), a polynomial fit to terrigenous sediments was used to derive the mass flux from physical erosion through the Phanerozoic. The mass flux through time was then normalized to the Miocene value to avoid the effect of extensive erosion from continental glaciation during the Pliocene and Quaternary and given a power-law relationship of 0.67. This was later updated (*72*) such that the normalized mass flux was first divided by 1.063 and then the power law was applied to provide an erosion parameter, which was included in the equations for silicate, organic carbon, and pyrite weathering. For NEOCARBSULF, we instead used reconstructed sediment mass fluxes (*73*), normalized to the Pleistocene to produce a minimum bound and to the Miocene to produce a maximum bound for our Monte Carlo simulation, and then applied a 100 million year moving average to both sets of bounds. Following previous work (*74*), we revised the power-law relationship for silicate, organic carbon, and pyrite weathering to be 0.33 and included erosion in the equations for carbonate weathering, which has been shown to have a more linear dependence (power-law relationship of 0.9).

### Rift and plate boundary modeling

Plate boundary lengths from 1000 Ma to the present are analyzed using a full-plate model that combines existing models that discretely cover the past 1000 million years (*75*). Rift events over the past 1000 million years were taken from prior work (*76*) for the Neoproterozoic as well as an earlier compilation (*77*) and digitized by others (*78*) for the Phanerozoic. These rifting events, which include failed rifts, are incorporated into the tectonic models as digitized polylines in GPlates (www.gplates.org). Subduction zone length was calculated using the pyGPlates python library (*76*). We also obtained the mantle to crust flux data from a previous study (their figure 4) (*79*). Each dataset (i.e., subduction zone lengths, rift lengths, and mantle to crust flux) is normalized to their present-day value, as per the original GEOCARBSULF (*38*) model, and the value for subduction zone lengths at 1000 Ma is extended back to 1600 Ma (1600 to 1500 Ma is the model spin-up time). In our Monte Carlo sampling for tectonic degassing, the lower boundary is obtained from the subduction zone lengths, while for the upper boundary we use either the rift length or the mantle to crust flux datasets, depending on which provides the highest value (generally the rift length data).

### Land area

The data for the land area ($f_A$) is the same as is used in previous modeling (*2*) for the Phanerozoic. For the Mesoproterozoic and Neoproterozoic, we derive land area values using crustal volume and thickness data (*80*) and the present-day crustal volume value (*81*).

### Carbon cycle changes

We modify the carbon cycle such that, instead of using the model-derived crustal carbon reservoir sizes in the weathering and degassing equations for young and ancient organic and carbonate carbon, as is the case with previous iterations of this type of model (*2*, *38*, *48*), we use the results generated previously (*79*), where they demonstrate that the crustal carbon inventory has increased steadily over time (Fig. 2D), which is an idea that has subsequently been explored by others (*82*). We normalized their results to their present-day value of $8500 \times 10^{18}$ moles and then multiplied this normalized value by the starting reservoir sizes of the different forms of carbon (see table S4), using the total crustal carbon value of $6250 \times 10^{18}$ moles from the original GEOCARBSULF (*38*). We have, however, changed the split of crustal carbon between inorganic and organic forms to be in the ratio of 0.23, instead of the prior 0.2 for the baseline model run. This allows various model processes, including atmospheric $O_2$, to finish the model run with present-day values but remains within the range permitted by a statistical analysis of the $\delta^{13}C$ record (*71*). The total amount of carbon in the model (i.e., the summation of all crustal reservoirs plus the ocean-atmosphere reservoir) is in mass balance through the entire model run time, but our changes to the carbon cycle alter the throughput of crustal carbon to the ocean-atmosphere reservoir by way of steadily increasing weathering and degassing fluxes through time (i.e., the system is not necessarily in steady state).

### Sulfur cycle changes

We introduce scaling factors (see Fig. 2, E and F, and the Supplementary Materials) to the following: the equation for gypsum burial (eq. S35) to simulate basin-scale evaporite deposition during the Tonian; the equations for young and ancient gypsum weathering (eqs. S19 and S20, respectively) to represent dissolution of the evaporite deposits during 560 to 580 Ma, roughly coincident with the Shuram-Wonoka anomaly; and to the equation for pyrite burial (eq. S34) during the Shuram-Wonoka anomaly, effectively turning a majority of the extra sulfate in the ocean, as a result of evaporite dissolution, into pyrite. This follows previous work (*50*) in exploring the idea that non–steady-state dynamics of the carbon cycle (i.e., the oxidation of a large pool of organic carbon) during the Neoproterozoic was supplemented by the $O_2$ produced during sulfate reduction to pyrite. This approach prevents the ocean-atmosphere becoming depleted in $O_2$ during the Shuram-Wonoka when the $\delta^{13}C$ record is extremely negative (see Fig. 2A).

### Monte Carlo setup

To capture some of the uncertainty in the model parameterization, we ran a Monte Carlo analysis of the NEOCARBSULF model, where a number of parameters were sampled from within defined limits, following a flat (instead of normal) distribution at each time step (see table S5). Although we varied 18 parameters in our main analysis, the three key parameters involved were the following: the $\delta^{13}C$ record (see Fig. 2A), which greatly influences the amount of $O_2$ produced by way of $C_{org}$ burial; the tectonic degassing ($f_G$) values used (Fig. 2B), which can change the amount of $O_2$ consumption from both pyrite and $C_{org}$ oxidation as well as the total carbon throughput; and mountain uplift ($f_R$; Fig. 2C), which, like tectonic degassing, affects $O_2$ consumption and total carbon throughput. The NEOCARBSULF model was run 5000 times instead of 10,000 times as used in previous modeling (*48*), as this was considered adequate for the number of parameters involved in this Monte Carlo simulation (see fig. S9 and associated text for further details).

## SUPPLEMENTARY MATERIALS

Supplementary material for this article is available at https://science.org/doi/10.1126/sciadv.abm8191

## REFERENCES AND NOTES

1. T. M. Lenton, T. W. Dahl, S. J. Daines, B. J. W. Mills, K. Ozaki, M. R. Saltzman, P. Porada, Earliest land plants created modern levels of atmospheric oxygen. *Proc. Natl. Acad. Sci. U.S.A.* **113**, 9704–9709 (2016).
2. A. J. Krause, B. J. W. Mills, S. Zhang, N. J. Planavsky, T. M. Lenton, S. W. Poulton, Stepwise oxygenation of the Paleozoic atmosphere. *Nat. Commun.* **9**, 4081 (2018).
3. L. J. Alcott, B. J. W. Mills, S. W. Poulton, Stepwise Earth oxygenation is an inherent property of global biogeochemical cycling. *Science* **366**, 1333–1337 (2019).
4. T. W. Lyons, C. T. Reinhard, N. J. Planavsky, The rise of oxygen in Earth's early ocean and atmosphere. *Nature* **506**, 307–315 (2014).
5. S. W. Poulton, A. Bekker, V. M. Cumming, A. L. Zerkle, D. E. Canfield, D. T. Johnston, A 200-million-year delay in permanent atmospheric oxygenation. *Nature* **592**, 232–236 (2021).
6. J. Farquhar, H. Bao, M. Thiemens, Atmospheric influence of earth's earliest sulfur cycle. *Science* **289**, 756–758 (2000).
7. K. Zahnle, M. Claire, D. Catling, The loss of mass-independent fractionation in sulfur due to a Palaeoproterozoic collapse of atmospheric methane. *Geobiology* **4**, 271–283 (2006).
8. S. J. Daines, B. J. W. Mills, T. M. Lenton, Atmospheric oxygen regulation at low Proterozoic levels by incomplete oxidative weathering of sedimentary organic carbon. *Nat. Commun.* **8**, 14379 (2017).
9. R. Buick, When did oxygenic photosynthesis evolve? *Philos. Trans. R. Soc. B Biol. Sci.* **363**, 2731–2743 (2008).
10. R. Rye, H. D. Holland, Paleosols and the evolution of atmospheric oxygen: A critical review. *Am. J. Sci.* **298**, 621–672 (1998).
11. H. D. Holland, The oxygenation of the atmosphere and oceans. *Philos. Trans. R. Soc. B Biol. Sci.* **361**, 903–915 (2006).
12. I. J. Glasspool, A. C. Scott, Phanerozoic concentrations of atmospheric oxygen reconstructed from sedimentary charcoal. *Nat. Geosci.* **3**, 627–630 (2010).
13. M. W. Wallace, A. Hood, A. Shuster, A. Greig, N. J. Planavsky, C. P. Reed, Oxygenation history of the Neoproterozoic to Early Phanerozoic and the rise of land plants. *Earth Planet. Sci. Lett.* **466**, 12–19 (2017).
14. D. A. Stolper, C. B. Keller, A record of deep-ocean dissolved $O_2$ from the oxidation state of iron in submarine basalts. *Nature* **553**, 323–327 (2018).
15. L. M. Och, G. A. Shields-Zhou, The Neoproterozoic oxygenation event: Environmental perturbations and biogeochemical cycling. *Earth Sci. Rev.* **110**, 26–57 (2012).
16. P. F. Hoffman, A. J. Kaufman, G. P. Halverson, D. P. Schrag, A neoproterozoic snowball earth. *Science* **281**, 1342–1346 (1998).
17. D. Wang, X. K. Zhu, N. Zhao, B. Yan, X. H. Li, F. Shi, F. Zhang, Timing of the termination of Sturtian glaciation: SIMS U-Pb zircon dating from South China. *J. Asian Earth Sci.* **177**, 287–294 (2019).
18. C. R. Calver, J. L. Crowley, M. T. D. Wingate, D. A. D. Evans, T. D. Raub, M. D. Schmitz, Globally synchronous marinoan deglaciation indicated by U-Pb geochronology of the cottons Breccia, Tasmania, Australia. *Geology* **41**, 1127–1130 (2013).
19. F. A. Macdonald, M. D. Schmitz, J. V. Strauss, G. P. Halverson, T. M. Gibson, A. Eyster, G. Cox, P. Mamrol, J. L. Crowley, Cryogenian of Yukon. *Precambrian Res.* **319**, 114–143 (2017).
20. G. M. Cox, V. Isakson, P. F. Hoffman, T. M. Gernon, M. D. Schmitz, S. Shahin, A. S. Collins, W. Preiss, M. L. Blades, R. N. Mitchell, A. Nordsvan, South Australian U-Pb zircon (CA-ID-TIMS) age supports globally synchronous Sturtian deglaciation. *Precambrian Res.* **315**, 257–263 (2018).
21. Z. X. Li, S. V. Bogdanova, A. S. Collins, A. Davidson, B. De Waele, R. E. Ernst, I. C. W. Fitzsimons, R. A. Fuck, D. P. Gladkochub, J. Jacobs, K. E. Karlstrom, S. Lu, L. M. Natapov, V. Pease, S. A. Pisarevsky, K. Thrane, V. Vernikovsky, Assembly, configuration, and break-up history of Rodinia: A synthesis. *Precambrian Res.* **160**, 179–210 (2008).

22. R. Frei, C. Gaucher, S. W. Poulton, D. E. Canfield, Fluctuations in Precambrian atmospheric oxygenation recorded by chromium isotopes. *Nature* **461**, 250–253 (2009).
23. N. J. Planavsky, C. T. Reinhard, X. Wang, D. Thomson, P. Mcgoldrick, R. H. Rainbird, T. Johnson, W. W. Fischer, T. W. Lyons, Low mid-Proterozoic atmospheric oxygen levels and the delayed rise of animals. *Science* **346**, 635–638 (2014).
24. D. B. Cole, C. T. Reinhard, X. Wang, B. Gueguen, G. P. Halverson, T. Gibson, M. S. W. Hodgskiss, N. R. Mckenzie, T. W. Lyons, N. J. Planavsky, A shale-hosted Cr isotope record of low atmospheric oxygen during the Proterozoic. *Geology* **44**, 555–558 (2016).
25. G. J. Gilleaudeau, R. Frei, A. J. Kaufman, L. C. Kah, K. Azmy, J. K. Bartley, P. Chernyavskiy, A. H. Knoll, Oxygenation of the mid-proterozoic atmosphere: Clues from chromium isotopes in carbonates. *Geochem. Perspect. Lett.* **2**, 178–187 (2016).
26. D. E. Canfield, S. Zhang, A. B. Frank, X. Wang, H. Wang, J. Su, Y. Ye, R. Frei, Highly fractionated chromium isotopes in Mesoproterozoic-aged shales and atmospheric oxygen. *Nat. Commun.* **9**, 2871 (2018).
27. N. J. Planavsky, C. T. Reinhard, T. T. Isson, K. Ozaki, P. W. Crockford, Large mass-independent oxygen isotope fractionations in mid-Proterozoic sediments: Evidence for a low-oxygen atmosphere? *Astrobiology* **20**, 628–636 (2020).
28. S. Zhang, X. Wang, H. Wang, C. J. Bjerrum, E. U. Hammarlund, M. M. Costa, J. N. Connelly, B. Zhang, J. Su, D. E. Canfield, Sufficient oxygen for animal respiration 1,400 million years ago. *Proc. Natl. Acad. Sci. U.S.A.* **113**, 1731–1736 (2016).
29. W. Lu, A. Ridgwell, E. Thomas, D. S. Hardisty, G. Luo, T. J. Algeo, M. R. Saltzman, B. C. Gill, Y. Shen, H. Ling, C. T. Edwards, M. T. Whalen, X. Zhou, K. M. Gutchess, L. Jin, R. E. M. Rickaby, H. C. Jenkyns, T. W. Lyons, T. M. Lenton, L. R. Kump, Z. Lu, Late inception of a resiliently oxygenated upper ocean. *Science* **361**, 174–177 (2018).
30. S. Wörndle, P. W. Crockford, M. Kunzmann, T. H. Bui, G. P. Halverson, Linking the bitter springs carbon isotope anomaly and Early Neoproterozoic oxygenation through I/[Ca + Mg] ratios. *Chem. Geol.* **524**, 119–135 (2019).
31. X. M. Liu, L. C. Kah, A. H. Knoll, H. Cui, C. Wang, A. Bekker, R. M. Hazen, A persistently low level of atmospheric oxygen in Earth's middle age. *Nat. Commun.* **12**, 351 (2021).
32. R. Tostevin, M. O. Clarkson, S. Gangl, G. A. Shields, R. A. Wood, F. Bowyer, A. M. Penny, C. H. Stirling, Uranium isotope evidence for an expansion of anoxia in terminal Ediacaran oceans. *Earth Planet. Sci. Lett.* **506**, 104–112 (2019).
33. P. A. E. Pogge von Strandmann, E. E. Stüeken, T. Elliott, S. W. Poulton, C. M. Dehler, D. E. Canfield, D. C. Catling, Selenium isotope evidence for progressive oxidation of the Neoproterozoic biosphere. *Nat. Commun.* **6**, 10157 (2015).
34. S. K. Sahoo, N. J. Planavsky, G. Jiang, B. Kendall, J. D. Owens, X. Wang, X. Shi, A. D. Anbar, T. W. Lyons, Oceanic oxygenation events in the anoxic Ediacaran ocean. *Geobiology* **14**, 457–468 (2016).
35. D. E. Canfield, S. W. Poulton, G. M. Narbonne, Late-Neoproterozoic deep-ocean oxygenation and the rise of animal life. *Science* **315**, 92–95 (2007).
36. D. E. Canfield, S. W. Poulton, A. H. Knoll, G. M. Narbonne, G. Ross, T. Goldberg, H. Strauss, Ferruginous conditions dominated later neoproterozoic deep-water chemistry. *Science* **321**, 949–952 (2008).
37. R. M. Garrels, A. Lerman, Coupling of the sedimentary sulfur and carbon cycles: An improved model. *Am. J. Sci.* **284**, 989–1007 (1984).
38. R. A. Berner, GEOCARBSULF: A combined model for Phanerozoic atmospheric $O_2$ and $CO_2$. *Geochim. Cosmochim. Acta* **70**, 5653–5664 (2006).
39. E. Tajika, in *The Extreme Proterozoic: Geology, Geochemistry, and Climate, Geophysical Monograph Series*, G. S. Jenkins, M. A. S. McMenamin, C. P. McKay, L. Sohl, Eds. (American Geophysical Union, Washington DC,2004), vol. 146, pp. 45–54.
40. D. H. Rothman, J. M. Hayes, R. E. Summons, Dynamics of the neoproterozoic carbon cycle. *Proc. Natl. Acad. Sci. U.S.A.* **100**, 8124–8129 (2003).
41. S. R. Schachat, C. C. Labandeira, M. R. Saltzman, B. D. Cramer, J. L. Payne, C. K. Boyce, Phanerozoic $pO_2$ and the early evolution of terrestrial animals. *Proc. R. Soc. B* **285**, 20172631 (2018).
42. E. A. Sperling, C. J. Wolock, A. S. Morgan, B. C. Gill, M. Kunzmann, G. P. Halverson, F. A. Macdonald, A. H. Knoll, D. T. Johnston, Statistical analysis of iron geochemical data suggests limited late proterozoic oxygenation. *Nature* **523**, 451–454 (2015).
43. J. A. Steadman, R. R. Large, N. J. Blamey, I. Mukherjee, R. Corkrey, L. V. Danyushevsky, V. Maslennikov, P. Hollings, G. Garven, U. Brand, C. Lécuyer, Evidence for elevated and variable atmospheric oxygen in the precambrian. *Precambrian Res.* **343**, 105722 (2020).
44. R. R. Large, I. Mukherjee, D. Gregory, J. Steadman, R. Corkrey, L. V. Danyushevsky, Atmosphere oxygen cycling through the proterozoic and phanerozoic. *Miner. Depos.* **54**, 485–506 (2019).
45. N. J. F. Blamey, U. Brand, J. Parnell, N. Spear, C. Lécuyer, K. Benison, F. Meng, P. Ni, Paradigm shift in determining Neoproterozoic atmospheric oxygen. *Geology* **44**, 651–654 (2016).
46. G. A. Shields, B. J. W. Mills, Tectonic controls on the long-term carbon isotope mass balance. *Proc. Natl. Acad. Sci. U.S.A.* **114**, 4318–4323 (2017).
47. B. Mills, T. M. Lenton, A. J. Watson, Proterozoic oxygen rise linked to shifting balance between seafloor and terrestrial weathering. *Proc. Natl. Acad. Sci. U.S.A.* **111**, 9073–9078 (2014).
48. D. L. Royer, Y. Donnadieu, J. Park, J. Kowalczyk, Y. Goddéris, Error analysis of $CO_2$ and $O_2$ estimates from the long-term geochemical model GEOCARBSULF. *Am. J. Sci.* **314**, 1259–1283 (2014).
49. S. Zhang, N. J. Planavsky, A. J. Krause, E. W. Bolton, B. J. W. Mills, Model based Paleozoic atmospheric oxygen estimates: A revisit to GEOCARBSULF. *Am. J. Sci.* **318**, 557–589 (2018).
50. G. A. Shields, B. J. W. Mills, M. Zhu, T. D. Raub, S. J. Daines, T. M. Lenton, Unique Neoproterozoic carbon isotope excursions sustained by coupled evaporite dissolution and pyrite burial. *Nat. Geosci.* **12**, 823–827 (2019).
51. G. P. Halverson, P. F. Hoffman, D. P. Schrag, A. C. Maloof, A. H. N. Rice, Toward a Neoproterozoic composite carbon-isotope record. *GSA Bull.* **117**, 1181–1207 (2005).
52. G. J. Gilleaudeau, S. J. Romaniello, G. Luo, A. J. Kaufman, F. Zhang, R. M. Klaebe, L. C. Kah, K. Azmy, J. K. Bartley, W. Zheng, A. H. Knoll, A. D. Anbar, Uranium isotope evidence for limited euxinia in mid-Proterozoic oceans. *Earth Planet. Sci. Lett.* **521**, 150–157 (2019).
53. K. V. Lau, F. A. Macdonald, K. Maher, J. L. Payne, Uranium isotope evidence for temporary ocean oxygenation in the aftermath of the Sturtian snowball Earth. *Earth Planet. Sci. Lett.* **458**, 282–292 (2017).
54. B. S. Gregory, M. W. Claire, S. Rugheimer, Photochemical modelling of atmospheric oxygen levels confirms two stable states. *Earth Planet. Sci. Lett.* **561**, 116818 (2021).
55. D. P. Schrag, J. A. Higgins, F. A. Macdonald, D. T. Johnston, Authigenic carbonate and the history of the global carbon cycle. *Science* **339**, 540–543 (2013).
56. C. Li, D. S. Hardisty, G. Luo, J. Huang, T. J. Algeo, M. Cheng, W. Shi, Z. An, J. Tong, S. Xie, N. Jiao, T. W. Lyons, Uncovering the spatial heterogeneity of Ediacaran carbon cycling. *Geobiology* **15**, 211–224 (2017).
57. L. A. Derry, A burial diagenesis origin for the Ediacaran Shuram-Wonoka carbon isotope anomaly. *Earth Planet. Sci. Lett.* **294**, 152–162 (2010).
58. J. M. Husson, B. J. Linzmeier, K. Kitajima, A. Ishida, A. C. Maloof, B. Schoene, S. E. Peters, J. W. Valley, Large isotopic variability at the micron-scale in "Shuram" excursion carbonates from South Australia. *Earth Planet. Sci. Lett.* **538**, 116211 (2020).
59. T. He, M. Zhu, B. J. W. Mills, P. M. Wynn, A. Y. Zhuravlev, R. Tostevin, P. A. E. Pogge von Strandmann, A. Yang, S. W. Poulton, G. A. Shields, Possible links between extreme oxygen perturbations and the Cambrian radiation of animals. *Nat. Geosci.* **12**, 468–474 (2019).
60. R. A. Berner, A model for atmospheric $CO_2$ over Phanerozoic time. *Am. J. Sci.* **291**, 339–376 (1991).
61. D. E. Canfield, J. Farquhar, Animal evolution, bioturbation, and the sulfate concentration of the oceans. *Proc. Natl. Acad. Sci. U.S.A.* **106**, 8123–8127 (2009).
62. T. J. Algeo, G. M. Luo, H. Y. Song, T. W. Lyons, D. E. Canfield, Reconstruction of secular variation in seawater sulfate concentrations. *Biogeosciences* **12**, 2131–2151 (2015).
63. M. Schidlowski, A 3,800-million-year isotopic record of life from carbon in sedimentary rocks. *Nature* **333**, 313–318 (1988).
64. R. A. Berner, Z. Kothavala, Geocarb III: A revised model of atmospheric $CO_2$ over Phanerozoic time. *Am. J. Sci.* **301**, 182–204 (2001).
65. T. W. Dahl, E. U. Hammarlund, A. D. Anbar, D. P. G. Bond, B. C. Gill, G. W. Gordon, A. H. Knoll, A. T. Nielsen, N. H. Schovsbo, D. E. Canfield, Devonian rise in atmospheric oxygen correlated to the radiations of terrestrial plants and large predatory fish. *Proc. Natl. Acad. Sci. U.S.A.* **107**, 17911–17915 (2010).
66. L. F. Shampine, M. W. Reichelt, The MATLAB ODE Suite. *SIAM J. Sci. Comput.* **18**, 1–22 (1997).
67. J. R. Havig, T. L. Hamilton, A. Bachan, L. R. Kump, Sulfur and carbon isotopic evidence for metabolic pathway evolution and a four-stepped Earth system progression across the Archean and Paleoproterozoic. *Earth Sci. Rev.* **174**, 1–21 (2017).
68. M. R. Saltzman, E. Thomas, in *The Geologic Time Scale 2012*, F. M. Gradstein, J. G. Ogg, M. D. Schmitz, G. M. Ogg, Eds. (Elsevier BV, 2012), vols. 1–2, pp. 207–232.
69. D. J. Beerling, J. A. Lake, R. A. Berner, L. J. Hickey, D. W. Taylor, D. L. Royer, Carbon isotope evidence implying high $O_2/CO_2$ ratios in the permo-carboniferous atmosphere. *Geochim. Cosmochim. Acta* **66**, 3757–3767 (2002).
70. R. A. Berner, S. T. Petsch, J. A. Lake, D. J. Beerling, B. N. Popp, R. S. Lane, E. A. Laws, M. B. Westley, N. Cassar, F. I. Woodward, W. P. Quick, Isotope fractionation and atmospheric oxygen: Implications for phanerozoic $O_2$ evolution. *Science* **287**, 1630–1633 (2000).
71. J. Krissansen-Totton, R. Buick, D. C. Catling, A statistical analysis of the carbon isotope record from the Archean to phanerozoic and implications for the rise of oxygen. *Am. J. Sci.* **315**, 275–316 (2015).
72. R. A. Berner, Addendum to "Inclusion of the Weathering of Volcanic Rocks in the GEOCARBSULF Model" (R. A. Berner, 2006, V. 306, p. 295–302). *Am. J. Sci.* **308**, 100–103 (2008).
73. W. W. Hay, A. Migdisov, A. N. Balukhovsky, C. N. Wold, S. Flögel, E. Söding, Evaporites and the salinity of the ocean during the Phanerozoic: Implications for climate, ocean circulation and life. *Palaeogeogr. Palaeoclimatol. Palaeoecol.* **240**, 3–46 (2006).
74. G. Li, H. Elderfield, Evolution of carbon cycle over the past 100 million years. *Geochim. Cosmochim. Acta* **103**, 11–25 (2013).

75. A. S. Merdith, S. E. Williams, A. S. Collins, M. G. Tetley, J. A. Mulder, M. L. Blades, A. Young, S. E. Armistead, J. Cannon, S. Zahirovic, R. D. Müller, Extending full-plate tectonic models into deep time: Linking the Neoproterozoic and the Phanerozoic. *Earth Sci. Rev.* **214**, 103477 (2021).
76. A. S. Merdith, S. E. Williams, S. Brune, A. S. Collins, R. D. Müller, Rift and plate boundary evolution across two supercontinent cycles. *Glob. Planet. Change* **173**, 1–14 (2019).
77. A. C. Şengör, B. A. Natal'in, Rifts of the world. *Geol. Soc. Am. Spec. Paper* **352**, 389–482 (2001).
78. S. Brune, S. E. Williams, R. D. Müller, Potential links between continental rifting, $CO_2$ degassing and climate change through time. *Nat. Geosci.* **10**, 941–946 (2017).
79. J. M. Hayes, J. R. Waldbauer, The carbon cycle and associated redox processes through time. *Philos. Trans. R. Soc. B Biol. Sci.* **361**, 931–950 (2006).
80. C. J. Hawkesworth, P. A. Cawood, B. Dhuime, Tectonics and crustal evolution. *Geol. Soc. Am. Today* **26**, 4–11 (2016).
81. G. Schubert, D. Sandwell, Crustal volumes of the continents and of oceanic and continental submarine plateaus. *Earth Planet. Sci. Lett.* **92**, 234–246 (1989).
82. C.-T. A. Lee, L. Y. Yeung, N. R. McKenzie, Y. Yokoyama, K. Ozaki, A. Lenardic, Two-step rise of atmospheric oxygen linked to the growth of continents. *Nat. Geosci.* **9**, 417–424 (2016).
83. D. E. Canfield, A new model for Proterozoic ocean chemistry. *Nature* **396**, 450–453 (1998).
84. D. E. Canfield, in *Treatise on Geochemistry*, H. D. Holland, K. K. Turekian, Eds. (Elsevier, ed. 2, 2014), pp. 197–216.
85. L. A. Levin, in *Oceanography and Marine Biology, An Annual Review*, R. N. Gibson, R. J. A. Atkinson, Eds. (CRC Press, 2003), p. 448.
86. C. M. Belcher, J. C. McElwain, Limits for combustion in low $O_2$ redefine Paleoatmospheric predictions for the Mesozoic. *Science* **321**, 1197–1200 (2008).
87. B. J. W. Mills, A. J. Krause, C. R. Scotese, D. J. Hill, G. A. Shields, T. M. Lenton, Modelling the long-term carbon cycle, atmospheric $CO_2$, and Earth surface temperature from Late Neoproterozoic to present day. *Gondw. Res.* **67**, 172–186 (2019).
88. J. K. G. Prince, R. H. Rainbird, B. A. Wing, Evaporite deposition in the mid-Neoproterozoic as a driver for changes in seawater chemistry and the biogeochemical cycle of sulfur. *Geology* **47**, 375–379 (2019).
89. J. Horita, H. Zimmermann, H. D. Holland, Chemical evolution of seawater during the Phanerozoic. *Geochim. Cosmochim. Acta* **66**, 3733–3756 (2002).
90. S. T. Brennan, T. K. Lowenstein, J. Horita, Seawater chemistry and the advent of biocalcification. *Geology* **32**, 473–476 (2004).
91. T. K. Lowenstein, M. N. Timofeeff, V. M. Kovalevych, J. Horita, The major-ion composition of Permian seawater. *Geochim. Cosmochim. Acta* **69**, 1701–1719 (2005).
92. B. C. Gill, T. W. Lyons, M. R. Saltzman, Parallel, high-resolution carbon and sulfur isotope records of the evolving Paleozoic marine sulfur reservoir. *Palaeogeogr. Palaeoclimatol. Palaeoecol.* **256**, 156–173 (2007).
93. N. Wu, J. Farquhar, H. Strauss, S. T. Kim, D. E. Canfield, Evaluating the S-isotope fractionation associated with Phanerozoic pyrite burial. *Geochim. Cosmochim. Acta* **74**, 2053–2071 (2010).
94. J. L. Payne, A. G. Boyer, J. H. Brown, S. Finnegan, M. Kowalewski, R. A. Krause, S. K. Lyons, C. R. McClain, D. W. McShea, P. M. Novack-Gottshall, F. A. Smith, J. A. Stempien, S. C. Wang, Two-phase increase in the maximum size of life over 3.5 billion years reflects biological innovation and environmental opportunity. *Proc. Natl. Acad. Sci. U.S.A.* **106**, 24–27 (2009).
95. A. J. Watson, thesis, University of Reading (1978).
96. C. M. Belcher, B. J. W. Mills, R. Vitali, S. J. Baker, T. M. Lenton, A. J. Watson, The rise of angiosperms strengthened fire feedbacks and improved the regulation of atmospheric oxygen. *Nat. Commun.* **12**, 503 (2021).
97. C. M. Belcher, M. E. Collinson, A. C. Scott, in *Fire Phenomena and the Earth System: An Interdisciplinary Guide to Fire Science*, C. M. Belcher, Ed. (Wiley-Blackwell, ed. 1, 2013), pp. 229–249.
98. S. Chang, R. A. Berner, Coal weathering and the geochemical carbon cycle. *Geochim. Cosmochim. Acta* **63**, 3301–3310 (1999).
99. R. A. Berner, Models for carbon and sulfur cycles and atmospheric oxygen: Application to paleozoic geologic history. *Am. J. Sci.* **287**, 177–196 (1987).
100. N. M. Bergman, T. M. Lenton, A. J. Watson, COPSE: A new model of biogeochemical cycling over phanerozoic time. *Am. J. Sci.* **304**, 397–437 (2004).
101. J. F. Kasting, What caused the rise of atmospheric $O_2$? *Chem. Geol.* **362**, 13–25 (2013).
102. S. H. Bottrell, R. J. Newton, Reconstruction of changes in global sulfur cycling from marine sulfate isotopes. *Earth Sci. Rev.* **75**, 59–83 (2006).
103. R. A. Berner, Burial of organic carbon and pyrite sulfur in the modern ocean: Its geochemical and environmental significance. *Am. J. Sci.* **282**, 451–473 (1982).
104. X. Hu, W. J. Cai, An assessment of ocean margin anaerobic processes on oceanic alkalinity budget. *Global Biogeochem. Cycles* **25**, GB3003 (2011).
105. L. R. Kump, R. M. Garrels, Modeling atmospheric $O_2$ in the global sedimentary redox cycle. *Am. J. Sci.* **286**, 337–360 (1986).
106. R. A. Berner, Phanerozoic atmospheric oxygen: New results using the geocarbsulf model. *Am. J. Sci.* **309**, 603–606 (2009).
107. R. A. Berner, GEOCARB II: A revised model of atmospheric $CO_2$ over phanerozoic time. *Am. J. Sci.* **294**, 56–91 (1994).
108. W. T. Holser, M. Schidlowski, F. T. Mackenzie, J. B. Maynard, in *Chemical Cycles in the Evolution of the Earth*, C. B. Gregor, R. M. Garrels, F. T. Mackenzie, J. B. Maynard, Eds. (Wiley, 1988), pp. 105–173.
109. Y. Goddéris, G. Le Hir, M. Macouin, Y. Donnadieu, L. Hubert-Théou, G. Dera, M. Aretz, F. Fluteau, Z. X. Li, G. P. Halverson, Paleogeographic forcing of the strontium isotopic cycle in the Neoproterozoic. *Gondw. Res.* **42**, 151–162 (2017).
110. T. M. Lenton, S. J. Daines, B. J. W. Mills, COPSE reloaded: An improved model of biogeochemical cycling over Phanerozoic time. *Earth Sci. Rev.* **178**, 1–28 (2018).
111. K. Caldeira, J. F. Kasting, The life span of the biosphere revisited. *Nature* **360**, 721–723 (1992).


**Acknowledgments:** We thank two anonymous reviewers for their constructive comments which helped to significantly improve the manuscript. **Funding:** This work is supported by the Natural Environment Research Council SPHERES Doctoral Training Partnership NE/L002574/1 (A.J.K.), UK Natural Environment Research Council NE/R010129/1 (B.J.W.M. and S.W.P.), UK Natural Environment Research Council NE/S009663/1 (B.J.W.M. and S.W.P.), Royal Society Wolfson Research Merit Award (S.W.P.), Leverhulme Research Fellowship (S.W.P.), Deep Energy Community of the Deep Carbon Observatory (A.S.M.), Richard Lounsbery Foundation (A.S.M.), MSCA-IF project 893615 (A.S.M.), and UK Natural Environment Research Council NE/P013651 (T.M.L.) **Author contributions:** Research design: A.J.K. and B.J.W.M. NEOCARBSULF modeling: A.J.K. Tectonic plate modeling: A.S.M. Writing: A.J.K., B.J.W.M., A.S.M., T.M.L., and S.W.P. **Competing interests:** The authors declare that they have no competing interests. **Data and materials availability:** The datasets required to run the model and the code for NEOCARBSULF, which is constructed in MATLAB, can be accessed via the DOI: 10.5281/zenodo.6954788 or can be found at https://github.com/Alexjkrause/NEOCARBSULF.

Submitted 13 October 2021
Accepted 25 August 2022
Published 14 October 2022
10.1126/sciadv.abm8191

Science Advances

# Extreme variability in atmospheric oxygen levels in the late Precambrian

Alexander J. KrauseBenjamin J. W. MillsAndrew S. MerdithTimothy M. LentonSimon W. Poulton

*Sci. Adv.*, 8 (41), eabm8191. • DOI: 10.1126/sciadv.abm8191